A new approach to measure momentum distributions and production cross sections of neutron rich nuclei using fragment separators

O. B. Tarasov[a,b], D. Bazin[a], T. Baumann[a], A. Gade[a,c], T.N. Ginter[a], M. Hausmann[a], D.J. Morrissey[a,d], J. Pereira[a], M. Portillo[a], B.M. Sherrill[a,c], A. Stolz[a], M. Thoennessen[a,c]

[a] *National Superconducting Cyclotron Laboratory, Michigan State University, East Lansing, MI 48824, USA*
[b] *Flerov Laboratory of Nuclear Reactions, JINR, 141980 Dubna, Moscow region, Russian Federation*
[c] *Department of Physics and Astronomy, Michigan State University, East Lansing, MI, USA 48824*
[d] *Department of Chemistry, Michigan State University, East Lansing, MI, USA 48824*

Abstract

The longitudinal momentum distributions of 34 neutron-rich isotopes of elements produced by fragmentation of a ^{76}Ge beam at 132 MeV/u with $13 \leq Z \leq 27$ were scanned using a novel experimental approach where a variety of targets with different thicknesses was used with the fragment separator at constant magnetic rigidity. In comparison to models that describe the shape and centroid of fragment momentum distributions, a parametrization based on the measured data was derived. Details of the transmission calculations, the analysis of their uncertainties, as well as the general analysis of momentum distributions and deduced cross sections obtained with this approach are presented.

Key words: Projectile fragmentation; Production cross sections; Longitudinal momentum distributions; Fragment separator; Two-stage separator; `LISE`$^{++}$ code
PACS: 24.10.-i; 25.70.Mn; 07.05.Tp

1. Introduction

Being able to predict the momentum distributions of residues when searching for new isotopes is important in order to optimize the fragment separator for the production of the most exotic isotopes. Also, accurate modeling of the momentum distributions allows for an estimation of the transmission and efficient suppression of contaminants. Several studies of parallel momentum distributions have been made, e.g. in [1, 2, 3, 4], but the predictions for the production of the most exotic nuclei are still very uncertain. A few semiempirical models [1, 2] used to describe the data assume Gaussian momentum distributions. These are characterized by two parameters (the mean value and the width), which may not be sufficient to fully model the momentum distributions. Therefore, measurements of the fragment momentum distributions remain an important task in the search for new isotopes.

In projectile fragmentation, the common way of measuring the momentum distributions of the fragments is to scan the magnetic rigidity ($B\rho$) with a fragment separator. A thin target is generally used to avoid complications from differential energy loss in the target (the systematic change in the kinetic energy lost by the projectile and residue nuclei in the target). The total cross section is determined by integrating these momentum distributions using a model or measurement of the angular transmission, as shown for example in Ref. [5].

In this work, a new approach to measure momentum distributions and cross sections (called "target scanning") is presented. In contrast to the so called "$B\rho$ scanning" method, typically using one thin target,

Email address: `tarasov@nscl.msu.edu` (O. B. Tarasov)

Table 1: Summary of experimental conditions used to measure isotope yields as described in the text. Targets and wedge are made from Be and Kapton, respectively. The momentum acceptance ($\Delta p/p$) and irradiation time were optimized for beam intensity and required statistical precision.

Data set	Fragment of interest	Target mg/cm^2	Wedge mg/cm^2	$\Delta p/p$ (%)	Time *hour*
1	^{43}S	9.8	-	0.1	1.0
2		97.5	-	0.1	2.0
3		191	-	0.1	2.0
4		288	-	0.1	1.9
5		404	-	0.1	0.9
6	^{43}S	191	20.2	1	3.4
7		288	20.2	2	6.0
8	^{66}V	404	20.2	5	19.9
9	^{54}Ar	629	20.2	5	9.4
10	^{59}Ca	629	20.2	5	21.6

a variety of targets with different thicknesses were used with a constant magnetic rigidity in the separator. In the case of very neutron-rich isotopes with low production, the "$B\rho$ scanning" method with a thin target is unpractical, whereas the "target scanning" method is particularly well suited to survey neutron-rich reaction residues. At a magnetic rigidity setting corresponding to the production of heavy neutron-rich nuclei, the lighter fragments have higher yields but will experience the largest differential energy loss, and hence, will fall outside the momentum acceptance of the separator with the thicker targets. Conversely, the heaviest fragments with the lowest yields will only be produced in sufficient numbers with the thickest targets but will experience lower differential energy losses and fall within the momentum acceptance.

In the present work, the longitudinal momentum distributions of 34 neutron-rich isotopes produced by fragmentation of a ^{76}Ge (132 MeV/u) with beryllium targets were scanned using a target scanning technique. Extensive simulations showed that this method can provide a sensitive measurement of the mean value and width of the momentum distributions. In this paper, we describe the details of this experimental approach, analyze its advantages and disadvantages compared to the classical "$B\rho$ scanning" method, and describe a procedure to estimate the transmission of fragments in order to extract the production cross sections.

2. Experiment

A 132 MeV/nucleon ^{76}Ge beam accelerated by the coupled cyclotrons at the NSCL was used to irradiate a series of ^{9}Be targets. The two-stage separator technique (A1900 fragment separator $\otimes$ S800 analysis beam line) described in Ref. [7] was used to select and identify reaction products. The details of the experimental set-up, detectors used, and the identification method of reaction products stopped in the Si telescope at the end of the S800 analysis beam line are described in Ref. [6].

The present experiment consisted of 10 runs in three parts that are summarized in Table 1. During all runs, the magnetic rigidity of the last two dipoles of the S800 analysis beam line was kept at 4.3 Tm, while the production target thickness was varied to effectively scan the momentum selection. This approach had the immediate advantage of greatly simplifing the particle identification during the runs.

The momentum acceptance of the A1900 fragment separator was restricted to $\Delta p/p = 0.1\%$ for the first part of the experiment devoted to the measurement of momentum distributions. The five different beryllium target thicknesses (listed in Table 1) allowed to probe the fragment momentum distributions for a large fraction of observed products, and subsequently extract their production cross sections.

In the second part of the experiment a Kapton achromatic degrader with a thickness of 20.2 mg/cm^2 was inserted at the dispersive image of the A1900 to reject less exotic fragments with an 8-mm aperture in the focal plane. The goal of this setting was to confirm the particle identification from part 1 using microsecond isomer tagging as described in Ref. [8]. The third and final part of the experiment was dedicated to the search for new isotopes and required the maximum momentum acceptance of the A1900, $\Delta p/p = 5.0\%$. Experimental data from the first part of the experiment was used to model the measured momentum distributions, and data from all three parts of the experiment were used to determine production cross sections.

3. Momentum distribution measurements with different targets at constant magnetic rigidity

The central results of the present work are the longitudinal momentum distributions of the projectile fragments. In this section we compare the advantages and disadvantages of target and "$B\rho$ scanning, report the results of detailed simulations, and present the experimental distributions for the example reaction.

3.1. Comparison of target scanning versus $B\rho$ scanning

The choice of momentum-measurement method is defined primarily by the goal of the experiment. A list of pros and cons for the two methods is given in Table 2. The $B\rho$ scanning method is better adapted to the study of reaction mechanisms that produce the highest cross sections, whereas our new target scanning method is well suited to the search for new isotopes and to improve the predictions of the momentum distributions of low cross sections.

Table 2: Comparison of momentum distribution measurement methods

Characteristics	$B\rho$ scanning $Thickness = const$	Target scanning $B\rho = const$
Fragment separator tuning for each measurement	yes	no
Particle identification for each measurement	at least should be verified	PID is constant
Number of measured distribution points	large	small
Number of measured isotopes	large	small
Measuring exotic nuclei (smallest cross sections)	difficult	straight forward
Contribution of energy loss in thick targets	small	large
Extracting longitudinal momentum distributions	straight forward	difficult
Applicable energy region	no restrictions	constant cross section region

Varying the target thickness in the target scanning method changes the energy of projectile by more than 25%, and therefore it is necessary to note that with this method we assume that the fragment production cross section and momentum distribution have small variations in this energy interval. For example, this method is not applicable in the energy region a little bit above the Fermi energy ($\sim$ 40 MeV/u), where the production cross sections change dramatically.

3.2. Simulations

A number of simulations have been carried out in order to illustrate the sensitivity of the momentum distribution characteristics to varying target thicknesses. The results were obtained for the present experimental conditions with the LISE^{++} code [9]. The rigidity of the last dipole was kept constant at 4.3 Tm while using the "Optimum target thickness" (thickness corresponding to maximum yield) routine to calculate production yields. Figure 1 shows the predicted yields for ^{42}S fragment from 132 MeV/u ^{76}Ge impinging on Be targets of thickness varying from 0 to 600 mg/cm^2. The momentum acceptance was restricted to $\Delta p/p = 0.1\%$ by slits at the dispersive focal plane of the first stage of the separator. Panels 1a and 1b show the predicted yields for a variety of models that specify the mean velocity and momentum distribution width value in the Laboratory frame for projectile fragmentation. The prescribed models and parametrization used are listed in Table 3. Note that the predicted peak positions can vary by as much as a factor of two between each other. The Goldhaber model [1] is used to predict the yields in the panels c-f. The middle panels show the target thickness dependence when the velocity ratio was fixed at $v/v_0 = 0.99$, and the width σ_0 ranged from 80 to 160 MeV/c. The thickness, at which the peak yield occurs, varies by almost 40% over the selected σ_0 range. The panels at the bottom illustrate the effect of varying the fragment-projectile velocity ratio v/v_0 from 0.96 to 1.0 and keeping the reduced width parameter σ_0 constant at the normally adopted value, 90 MeV/c. In this velocity ratio region, the target thickness at which the distribution peaks varies by a factor of three. This demonstrates how sensitive the optimum target thickness is to the models and their parametrizations. It is necessary to minimize the number and range of target thicknesses used during such a measurement. The shape and peak of the longitudinal momentum distribution is critical in determining the cross section from the yield, hence one needs to establish which model best describes the experimental observations.

Table 3: Momentum distribution models used in the LISE^{++} calculations presented in Fig. 1 (a) and (b).

Label	Velocity ratio (v/v_0)	Distribution Width
B+G	[10] (V.Borrel et al.)	[1] (A.S.Goldhaber)
1+G	$v/v_0 = 1$	[1] (A.S.Goldhaber)
Mor	[2] (D.J.Morrissey)	
Tar	[4] (O.B.Tarasov)	

3.3. Analysis procedure

A systematic approach is used in the present work to determine the optimum set of parameters for the models described above, and make reasonable predictions of the measured yields versus target thickness. As indicated for the five targets listed in Table 1, the yields of various isotopes were measured with the fragment separator set to 4.3 Tm. The isotopes within the $B\rho$ selection of the fragment separator are determined by the relation:

$$A/q \sim B\rho/(\beta\gamma), \tag{1}$$

where A and q are the mass and charge of the fragment, and $\beta = v/c$, $\gamma = (1-\beta^2)^{-1/2}$. This magnetic rigidity value was chosen such that the ^{43}S yield is optimal over the target scan. The momentum distributions for 34 isotopes located near the line $A = 2.56\ q + 1.6$ were measured and reconstructed to deduce the cross sections. The 8 highest yields from ^{35}Al to ^{70}Co shown in Fig. 2 as a function of the velocity ratio were fitted with Gaussian functions in order to deduce the production cross sections. It should be noted that at the energy of this experiment, the shape of the fragment momentum distribution (presented as the normalized velocity distribution in Fig. 2) is asymmetric due to a low-energy exponential tail thought to be due to dissipative processes [4]. The Gaussian function used for the present data does not take this tail into account, but the underestimation of the cross section is small ($\sim 1 - 2\%$).

The measured yields of selected isotopes are shown as a function of target thickness in Fig. 3. The yields calculated with LISE^{++}using parameters from Morrissey's model of the reaction and EPAX cross sections [11]

Table 4: Parameters of the Convolution model [4] used in LISE^{++} calculations presented in Fig. 4

#	Separation energy	coefficient	shift
0	Q_g	3.344	0.158
1	E_S	2.4	0.149
2	$Q_g + E_S$	2.936	0.153
$\sigma_0^{conv} = 91 MeV/c$			

are indicated by the dashed lines. The yields obtained with experimental parameters – area (cross section), velocity ratio (v/v_0), width (σ_0) – from fitting the velocity distributions (see Fig. 2) are shown by the solid lines in Fig. 3. Figure 3 demonstrates the agreement between experimental data and calculations with parameters produced by fitting the velocity distributions. It also demonstrates the capability of this new method to study momentum distributions, without complications due to energy loss contributions in thick targets.

4. Results and Discussion

4.1. Momentum distribution model for neutron-rich isotopes with $13 \leq Z \leq 27$

The results of fitting the velocity distributions (Fig. 2) are presented in Fig. 4 (velocity ratio – v/v_0) and Fig. 5 (reduced width – σ_0 [MeV/c]). A survey of all of the fitted results shows that fragments are produced with slightly broader momentum distributions in the heavy ($35 \leq A \leq 70$) mass region and significantly higher velocities in the region of mass $35 \leq A \leq 55$ than the Morrissey model predictions. This model assumes that the energy necessary to remove each nucleon is $E_S = 8$ MeV, a value derived for fragments close to stability. Neutron-rich nuclei are less bound, which could explain their higher velocities than compared to stable nuclei. Further analysis shows (see Fig. 6) that the separation energy parameter for nuclei observed in the present work in the region $A_P/2 \leq A_F \leq A_P$ exhibits a linear decrease with the number of removed nucleons:

$$E_S = 8 - 11.2\Delta A/A_P, \tag{2}$$

where $\Delta A = A_P - A_F$, A_P is the projectile mass number, and A_F is the fragment mass number.

Although the convolution model (Fig. 4, #1) [4] gives a good agreement for the fragment velocities, the calculated widths are narrower than experimentally observed. The formulae used in the convolution model are too complicated to fit the experimental data due to the large number of parameters. It was therefore decided to use the Morrissey model for the following transmission calculations using the newly obtained parameters E_S for the velocity ratio calculations, and the reduced width parameter $\sigma_0 = 105 \pm 15$ MeV/c obtained from Fig. 5.

4.2. Transmission calculation

The inclusive production cross sections for the observed fragments were calculated by correcting the measured yields for the finite longitudinal-momentum and angular acceptances of the separator system. A total of thirty-four cross sections were obtained from Gaussian functions fitted to the longitudinal momentum distributions. The cross sections for the remaining fragments with incomplete longitudinal momentum distributions were obtained with estimated transmission corrections.

In order to estimate the systematic errors in the transmission corrections, the angular, longitudinal, and wedge selection transmissions were calculated with different parameters (see Table 5) for each isotope in each experimental setting (see Table 1), using the Morrissey model [2] of momentum distributions with parameters (E_S, σ_0) as described above. The wedge transmission corresponds to the fraction of isotopes that pass through the slits at the focal plane when the wedge is inserted at the intermediate dispersive image.

The first LISE^{++} calculation (see Table 5) was used to estimate the total fragment transmission including losses due to reactions of the fragment with the target and the wedge. Then by varying the parameters

Table 5: List of LISE^{++} calculations used to estimate systematic transmission errors.

No.	Goal	Parameters		
		Reduced $P_{\|}$ width, σ_0 (MeV/c)	Angular acceptance (msr)	FP slit (mm)
1	total transmission	**105**	**8.2**	**8**
2	momentum	**120**	8.2	8
3	transmission error	**90**	8.2	8
4	angular	105	**6.6**	8
5	transmission error	105	**9.9**	8
6	wedge	105	8.2	**6**
7	transmission error	105	8.2	**10**

Table 6: Transmissions of fragments of interest in the data sets with a wedge.

Data set	Fragment	Transmission(%)			
		Momentum	Angular	Wedge	Total
6	^{43}S	11 ± 3	$70\ ^{+7}_{-8}$	$75\ ^{+10}_{-14}$	6 ± 2
7	^{43}S	16 ± 3	$69\ ^{+7}_{-8}$	$74\ ^{+10}_{-14}$	8 ± 2
8	^{66}V	70 ± 3	$99\ ^{+1}_{-2}$	$83\ ^{+8}_{-13}$	$58\ ^{+6}_{-10}$
9	^{54}Ar	30 ± 3	$86\ ^{+8}_{-6}$	$78\ ^{+10}_{-14}$	$20\ ^{+3}_{-4}$
10	^{59}Ca	32 ± 3	$93\ ^{+3}_{-5}$	$80\ ^{+9}_{-14}$	$24\ ^{+3}_{-5}$

as shown in Table 5, transmission uncertainties have been calculated. The estimate of the uncertainties in the momentum transmission come from the one-sigma limits of the reduced width ($\pm$15 MeV/c). For the angular transmission an angular acceptance uncertainty of $\pm$5 mrad was used for horizontal and vertical directions. The effective wedge selection slit size was experimentally obtained to be 8 ± 2 mm. For example, the values of the angular, momentum, wedge, and overall transmissions for the fragment of interest in runs with a wedge are given in Table 6. The calculated transmissions of Argon isotopes for the data set #9 (see Table 1) are given in Table 7.

It is clear from Table 6 that the momentum transmission uncertainty dominates for light isotopes with small momentum acceptance $\leq 2\%$ ($\sim 30\%$ relative error), whereas the wedge selection uncertainty dominates for heavier isotopes ($\sim 15\%$) with the full A1900 momentum acceptance.

4.3. Experimental uncertainties

The errors in the fragmentation cross sections are calculated based on statistical, transmission systematic, and data-set systematic uncertainties. The transmission uncertainties depend on the momentum distribution model, wedge transmission (at the focal plane slits), and angular acceptance uncertainties, as discussed in the previous section. The data set systematic uncertainties depend on the integrated beam current, the target thickness, and the momentum selection slit uncertainties given in Table 8.

For the target thickness, an uncertainty of half of the variation between two thickness measurements was used. The first measurement was done with a micrometer using the known density of the material. Measuring the position of the primary beam in the A1900 dispersive plane after passing through a target, an target thickness was obtained using energy loss calculations, which provided the second measurement.

The uncertainty of the momentum slit size was calculated based on the uncertainty of slit position and scattering of fragments at the slit edges. The dispersion uncertainty can be expressed as uncertainty of the effective slit width. This uncertainty was added as well to the uncertainty of the slit size. The momentum slit size uncertainty only impacts settings with a small momentum acceptance. For large momentum acceptances

Table 7: Calculated transmissions of Argon isotopes for the data set #9 (see Table 1) with a wedge. The two-stage separator has been tuned on ^{54}Ar.

	Transmission(%)			
Isotope	Momentum	Angular	Wedge	Total
^{49}Ar	$1.2\ ^{+0.4}_{-0.5}$	$76\ ^{+13}_{-8}$	$30\ ^{+11}_{-10}$	$0.3\ ^{+0.2}_{-0.1}$
^{50}Ar	$4.8\ ^{+0.3}_{-0.7}$	$78\ ^{+12}_{-7}$	42 ± 12	1.6 ± 0.5
^{51}Ar	14 ± 1	$80\ ^{+11}_{-7}$	$54\ ^{+12}_{-13}$	6 ± 2
^{52}Ar	24 ± 3	$83\ ^{+10}_{-7}$	$67\ ^{+11}_{-14}$	13 ± 3
^{53}Ar	30 ± 3	$84\ ^{+9}_{-6}$	$75\ ^{+10}_{-14}$	19 ± 4
^{54}Ar	30 ± 3	$86\ ^{+8}_{-6}$	$78\ ^{+10}_{-14}$	$20\ ^{+3}_{-4}$
^{55}Ar	$29\ ^{+2}_{-3}$	$88\ ^{+8}_{-6}$	$74\ ^{+10}_{-14}$	$19\ ^{+3}_{-4}$
^{56}Ar	26 ± 2	$89\ ^{+7}_{-6}$	$63\ ^{+12}_{-14}$	$15\ ^{+3}_{-4}$

Table 8: Data set systematic uncertainties and data acquisition live time (all values in %).

Data set	Target thickness	Momentum slits	Beam particles	Live time
1	3.9	8.9	1.03	94.3
2	1.0	8.9	1.03	95.1
3	1.5	8.9	1.03	91.9
4	1.3	8.9	1.03	93.9
5	1.4	8.9	1.03	94.9
6	1.5	1.9	1.03	92.2
7	1.3	1.7	1.03	88.9
8	1.4	1.7	1.03	99.7
9	1.2	1.7	1.03	99.7
10	1.2	1.7	1.03	99.6

the momentum transmission uncertainty dominates (see the previous section). For the beam particles uncertainty, the relative deviation (1.03%) between the calibration line and experimental values was used.

Systematic uncertainties are dominant in the case of thin targets with a small momentum acceptance and without wedge. The uncertainties in other data sets (#6-10) with large momentum acceptances are dominated by the transmission uncertainties.

4.4. Production cross sections

The production cross sections for ^{40}P, ^{47}Ar, ^{56}Ca, and ^{62}V fragments from the reaction of ^{76}Ge with beryllium targets are shown in Fig. 7. The cross sections deduced for each data set are based on LISE^{++} transmission calculations using model [2] of the momentum distribution and the new parameters E_S and σ_0 as described before. They are used to obtain an average-weighted value, labeled "Average" cross section. As can be seen in Fig. 7, the fluctuations between data set cross sections are small. Only two points with large uncertainties (data set #9 for ^{40}P and data set #7 for ^{62}V) are located significantly below the average. Both of these points correspond to very low momentum transmission ($< 0.2\%$) and due to the large transmission uncertainties they do not contribute to the final weighted averages. We would like to add, that similar experimental points obtained on the tails of momentum distributions with very small momentum transmissions should be eliminated.

A total of 34 cross sections with beryllium targets were obtained from Gaussian functions fitted to the longitudinal momentum distributions. The weighted average cross sections are consistent with the cross sections obtained by integration of the momentum distributions. This demonstrates the quality of the transmission calculations with the chosen model.

The cross sections obtained for all of the fragments observed in this experiment were presented in Fig. 8 of Ref. [6] along with the predictions of the `EPAX` parametrization, and the model-based cross sections were found to be in good agreement with those produced by integrating the measured longitudinal momentum distributions.

5. Summary

The momentum distributions and cross sections for a large number of neutron-rich nuclei produced by the ^{76}Ge beam were measured by varying the target thickness in a two-stage fragment separator with a fixed momentum acceptance. Extensive simulations showed that this new approach can provide a sensitive measurement of the mean value and width of the momentum distribution of neutron-rich nuclei. The longitudinal momentum distributions of 34 neutron-rich isotopes of the elements with $13 \leq Z \leq 27$ were produced. New parameters for the momentum distribution model [2] based on the measured momenta were obtained.

References

[1] A. S. Goldhaber, Phys. Lett. B 53 (1974) 306.
[2] D. J. Morrissey, Phys. Rev. C 39 (2) (1989) 460.
[3] R. Pfaff, D. J. Morrissey, M. Fauerbach, M. Hellström, J. H. Kelley, R. A. Kryger, B. M. Sherrill, M. Steiner, J. S. Winfield, J. A. Winger, S. J. Yennello, B. M. Young, Phys. Rev. C 51 (1995) 1348.
[4] O. Tarasov, Nucl. Phys. A 734 (2004) 536.
[5] M. Fauerbach, D. J. Morrissey, W. Benenson, B. A. Brown, M. Hellström, J. H. Kelley, R. A. Kryger, R. Pfaff, C. F. Powell, B. M. Sherrill, Phys. Rev. C 53 (1996) 647.
[6] O. B. Tarasov, M. Portillo, A. M. Amthor, T. Baumann, D. Bazin, A. Gade, T. N. Ginter, M. Hausmann, N. Inabe, T. Kubo, D. J. Morrissey, A. Nettleton, J. Pereira, B. M. Sherrill, A. Stolz, M. Thoennessen, Phys. Rev. C 80 (2009) 034609.
[7] T. Baumann, A. M. Amthor, D. Bazin, B. A. Brown, C. M. Folden III, A. Gade, T. N. Ginter, M. Hausmann, M. Matos, D. J. Morrissey, M. Portillo, A. Schiller, B. M. Sherrill, A. Stolz, O. B. Tarasov, M. Thoennessen, Nature 442 (2007) 1022.
[8] R. Grzywacz, R. Anne, G. Auger, D. Bazin, C. Borcea, V. Borrel, J. M. Corre, T. Dorfler, A.Fomichov, M. Gaelens, D. Guillemaud-Mueller, R. Hue, M. Huyse, Z. Janas, H. Keller, M. Lewitowicz, S. Lukyanov, A. C. Mueller, Y. Penionzhkevich, M. Pfutzner, F. Pougheon, K. Rykaczewski, M. G. Saint-Laurent, K. Schmidt, W.-D. Schmidt-Ott, O. Sorlin, J. Szerypo, O. Tarasov, J. Wauters, J. Zylicz, Phys. Lett. B 355 (1995) 439.
[9] O. B. Tarasov and D. Bazin, Nucl. Inst. Meth. Phys. Res. B 266 (2008) 4657;
available at: `http:\\www.nscl.msu.edu\lise`
[10] V. Borrel, D. Guerreau, J. Galin, B. Gatty, D. Jacquet, X. Tarrago, Z. Phys. A 314 (1983) 191.
[11] K. Sümmerer and B. Blank, Phys. Rev. C 61 (2000) 034607.

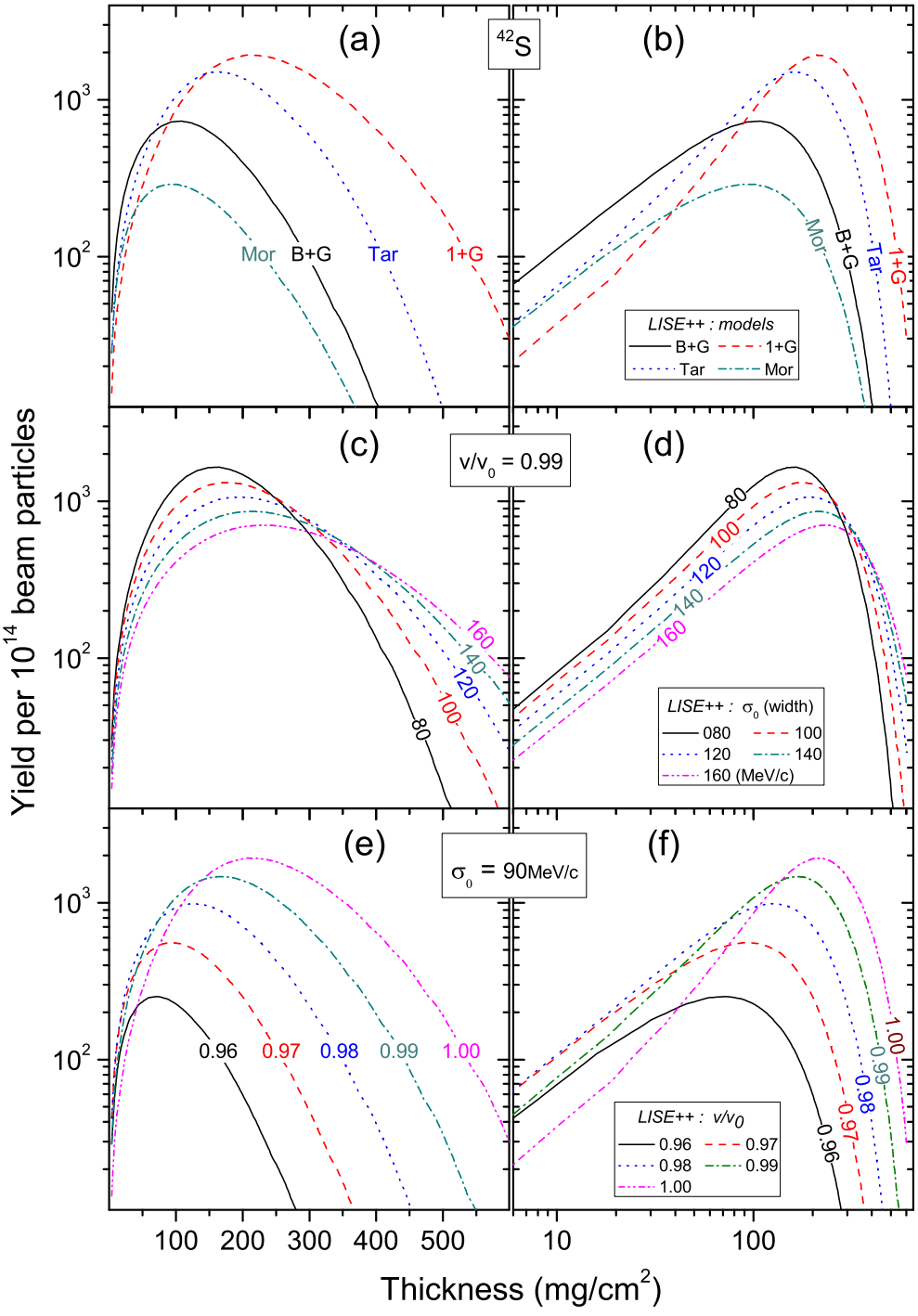

Figure 1: (Color online) ^{42}S yield calculated by LISE^{++} [9] versus Be target thickness from a ^{76}Ge beam as described in the text. Note that the left panels have a linear horizontal scale, while the right panels have a logarithmic scale to emphasize the difference between calculated curves for the thick and thin targets. See text for the meaning of the different lines.

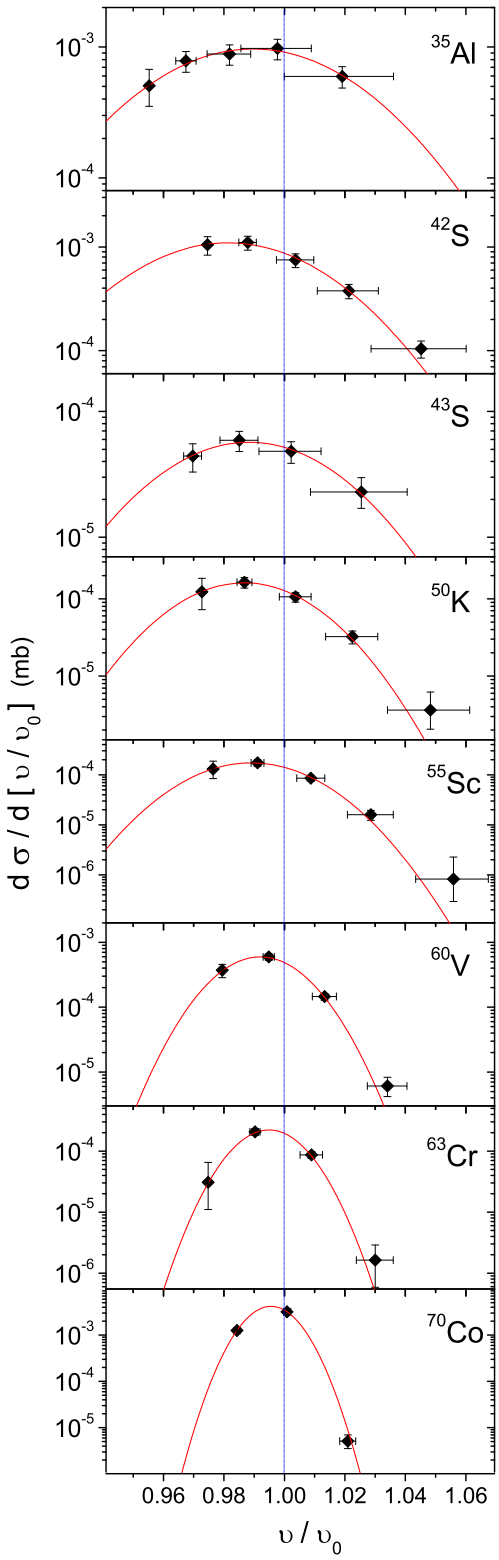

Figure 2: (Color online) Differential cross sections of ^{35}Al, ^{42}S, ^{43}S, ^{50}K, ^{55}Sc, ^{60}V, ^{63}Cr, and ^{70}Co fragments obtained for different target thickness at constant magnetic rigidity. The solid lines represent the fitted Gaussian functions. The horizontal error bars correspond to the velocity difference between production at the beginning or the end of the target.

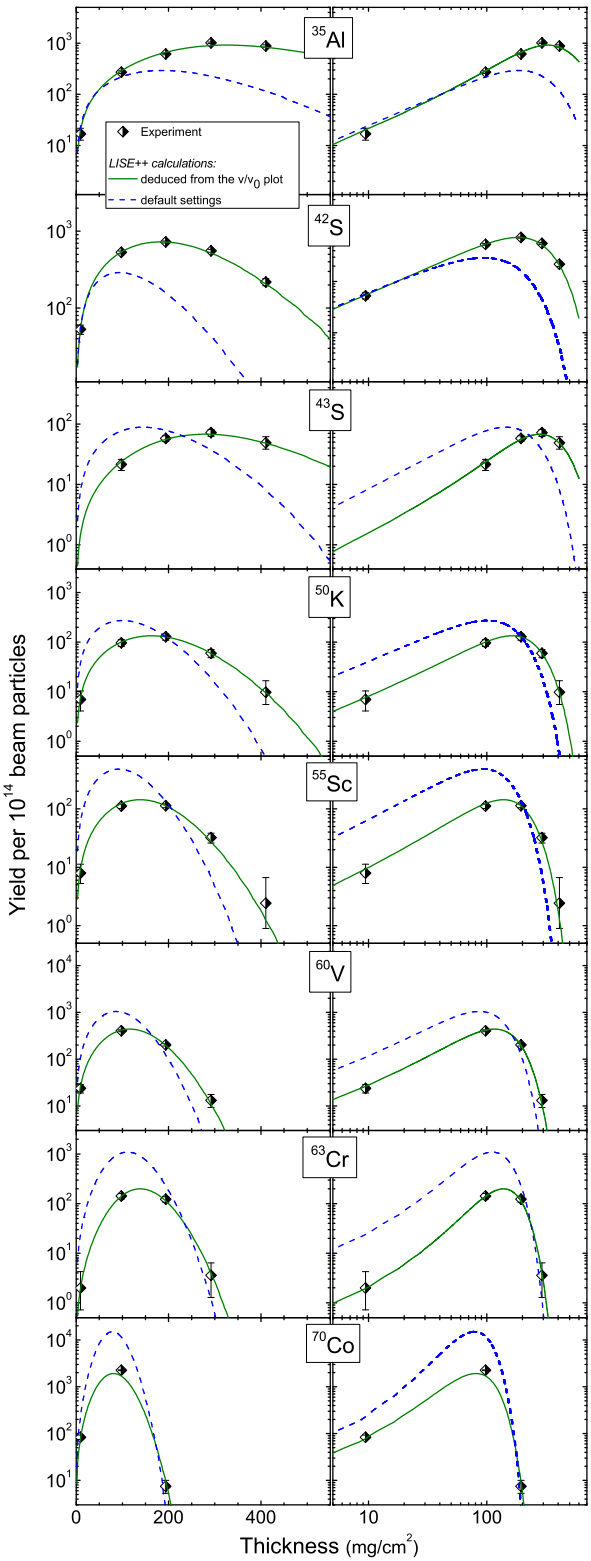

Figure 3: (Color online) Measured yield of ^{35}Al, ^{42}S, ^{43}S, ^{50}K, ^{55}Sc, ^{60}V, ^{63}Cr, and ^{70}Co as function of target thickness. The lines show the LISE^{++} calculations with parameters deduced from fitting the velocity distributions shown in Fig. 2 (green solid line) and default model settings [2] (blue dashed line) as described in the text.

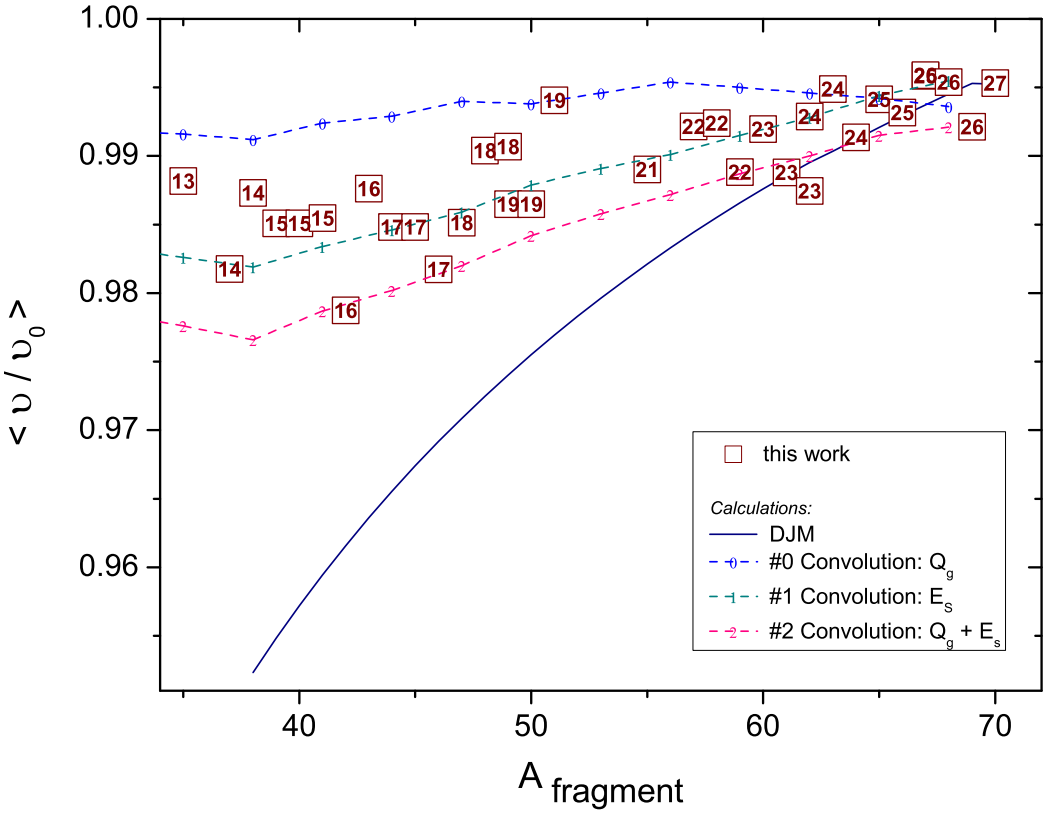

Figure 4: (Color online) Experimental mean ratios of the fragment velocities to the projectile velocity for neutron-rich isotopes (located along the line $A = 2.56\ q + 1.6$) produced by fragmentation of a ^{76}Ge beam at 132 MeV/u with beryllium targets. The atomic numbers are shown inside of rectangles. The solid line represents calculations using D.J.Morrissey's model [2] with default settings ($\sigma_0 = 87$ MeV/c, $E_S = 8$ MeV). See text for details. The dashed lines represent the convolution model results with separation energy modes as listed in Table 4.

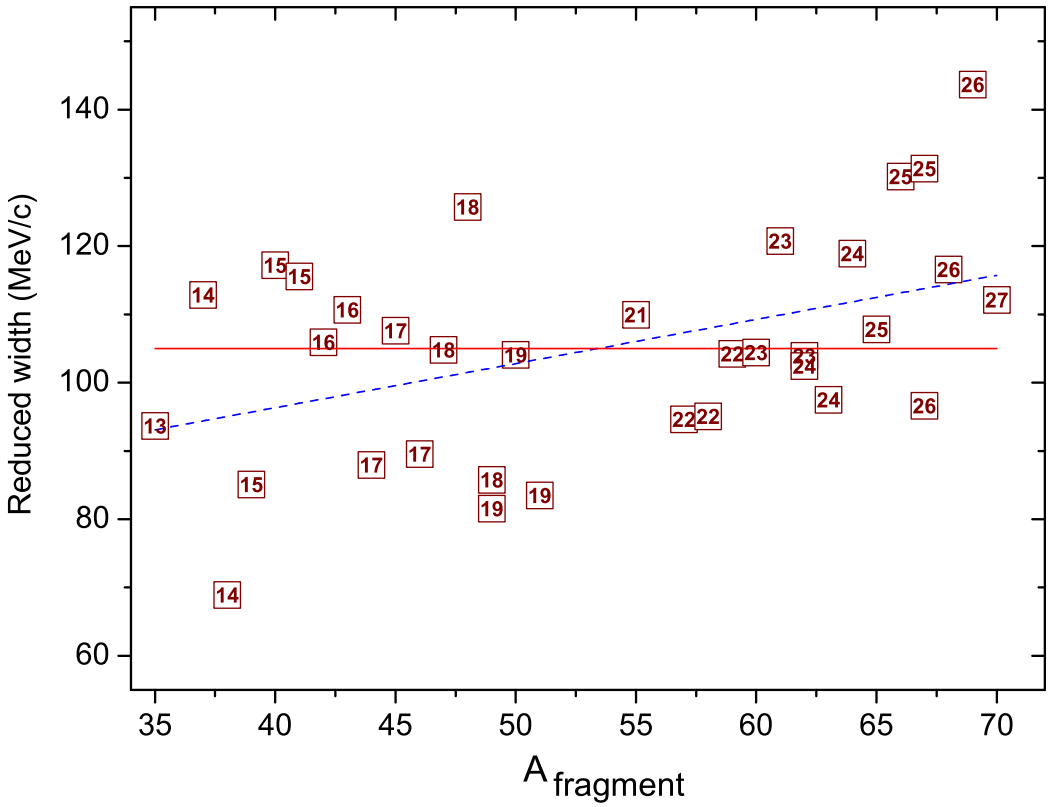

Figure 5: (Color online) Momentum distribution reduced widths for the model in Ref. [2] are plotted as a function of fragment mass. The atomic numbers are shown inside of rectangles. The blue dashed line shows the result of a linear fit ($\sigma_0 = 70.5 + 0.65A_f$), and the red solid line show the best constant value ($\sigma_0 = 105$ MeV/c).

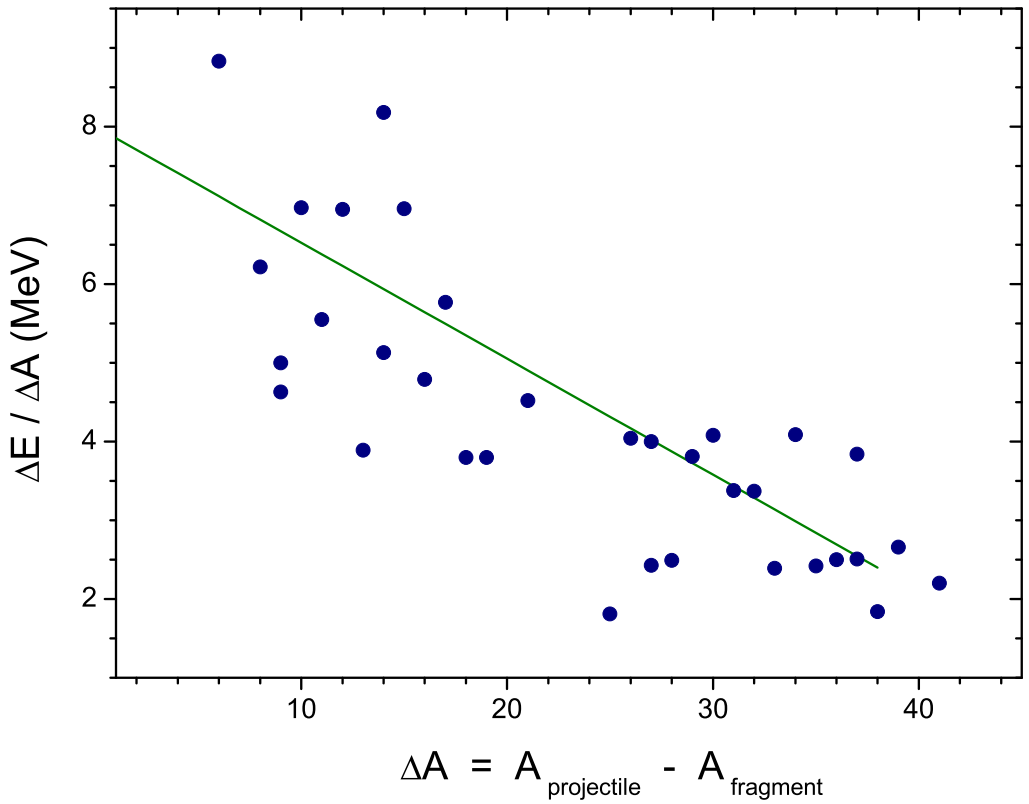

Figure 6: (Color online) Separation energy values ($E_S = \Delta E/\Delta A$) for Morrissey's model deduced from the experimental data shown in Fig. 2 . Values are plotted as a function of the number of removed nucleons ($\Delta A = A_P - A_F$). The solid line represents a linear fit ($E_S = 8 - 11.2\Delta A/A_P$).

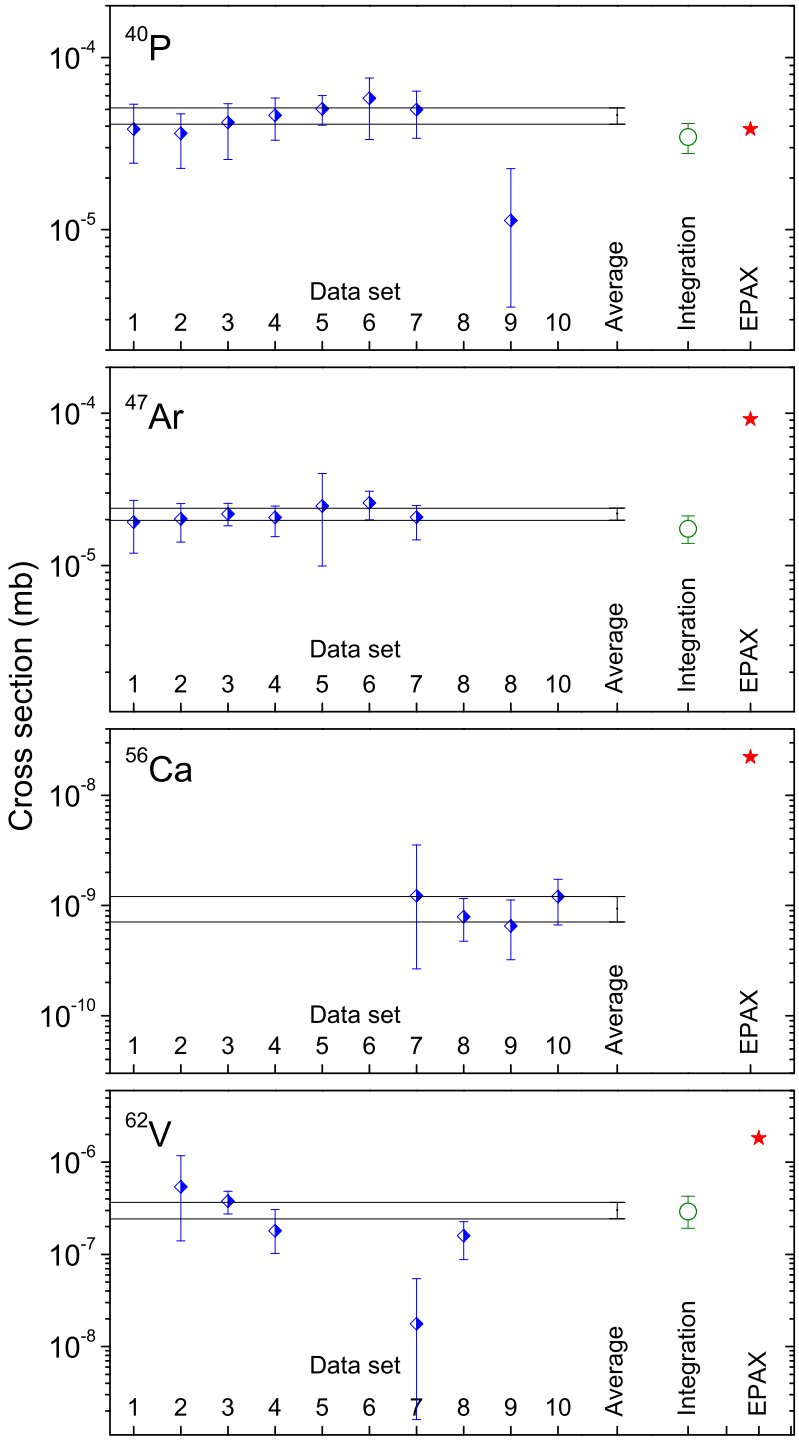

Figure 7: (Color online) Production cross sections for ^{40}P, ^{47}Ar, ^{56}Ca, and ^{62}V fragments from the reaction of ^{76}Ge with beryllium targets. The blue semi-solid diamonds represent the cross sections based on LISE^{++} transmission calculations with model [2] of the momentum distribution using newly determined parameters E_S and σ_0. The black solid horizontal lines shows the upper and lower limits of their average weighted values. The cross sections obtained by integration of the momentum distributions are shown by the open green circles, where sufficient data was available. The red stars show the predictions of the EPAX systematics.